6 Laboratory testing of rocks

6.1 Introduction

The mechanical properties of a piece of rock depend on its mineral composition, the arrangement of the mineral grains, and any cracks that may have been introduced into it during its long geological history by diagenesis or tectonic forces. Consequently, the mechanical properties of rock vary not only between different rock types but also between different specimens of the nominally same rock. Hence, unlike "reproducible" engineering materials such as steels, for which property values can be measured on standard specimens and listed in handbooks, only very rough approximate values of the mechanical properties of a given rock can be estimated from tabulated handbook data. For this reason, laboratory testing necessarily plays a large role in rock mechanics.

In this chapter we describe the basic types of laboratory measurements that are routinely conducted to measure the mechanical properties of rocks. Each particular experimental apparatus and/or procedure subjects the rock specimen to a certain state of stress. The chapter is structured in such a way that successively more complex stress states are considered in each subsequent section. We start in §6.2 with a discussion of hydrostatic tests that can be performed on porous rocks. Uniaxial compression tests are discussed in §6.3. Traditional triaxial compression tests, in which the two lateral stresses are equal to each other and less than the axial stress, are discussed in §6.4. The effect of the mechanical stiffness of the testing machine is examined in §6.5. True-triaxial, or polyaxial tests, in which three different stresses may be applied to the sample, are discussed in §6.6. In all of the aforementioned tests, the stress state induced in the sample is nominally homogeneous.

There are several other important test configurations in which an inhomogeneous state of stress is induced in the rock. The so-called "Brazilian test," which is used to create a tensile stress within a rock, is described in §6.7. Torsion of a cylindrical specimen is discussed in §6.8, along with the mathematical solution for the stresses and displacements. Bending of a beam-like specimen is treated in §6.9, again along with a brief mathematical derivation of the stresses and displacements. Finally, compression tests on hollow cylinders are discussed in §6.10.

In each case, the discussion will be quite general, focusing on the salient features of the experimental apparatus, the state of stress involved in the tests,

and the interpretation of the test results for the purpose of extracting numerical values of the relevant rock properties. More specific details of the design of the apparatuses, and other technical issues that arise during these tests, can be found in several major review articles, such as Tullis and Tullis (1986). Specifications of standard testing procedures and practices, such as specimen size, suggested strain rates, etc., can be found in the various "ISRM Suggested Methods," which are prepared under the authority of the International Society for Rock Mechanics and published in the *International Journal of Rock Mechanics and Mining Sciences*.

Although the focus will be on describing the measurement systems and procedures, some representative data will be discussed. Many data sets on rock deformation were originally measured using British Imperial units, with stresses measured in pounds per square inch (psi). Such units are still used in some countries and within the petroleum industry. Geophysicists, on the other hand, usually quantify stresses in units of bars. Modern scientific convention, as codified in the Système Internationale (SI), requires stresses to be measured in Pascals, defined by $1\ \text{Pa} = 1\ \text{N/m}^2$. Conversion between these units can be achieved through the relations $1\ \text{psi} = 6895\ \text{Pa}$, $1\ \text{bar} = 10^5\ \text{Pa}$.

6.2 Hydrostatic tests

The simplest type of boundary traction that can be applied to the outer boundary of a piece of rock is a uniform normal traction, such as would be exerted if the boundary of the rock were in contact with a fluid. In a homogeneous solid, such boundary conditions would give rise to a state of uniform hydrostatic stress throughout the body. The ratio of the magnitude of the stress to the volumetric strain of the sample would then, according to (5.7), give the bulk modulus K of the rock.

This type of test can be conducted in a pressure vessel filled with a pressurized fluid (Fig. 6.1). The pressurizing fluid is connected to a pump or piston located outside the pressure cell. The pressure of the fluid, also referred to as the *confining pressure*, is measured by a manual pressure gauge or electronic pressure transducer. As there will be no pressure gradient in the fluid, aside from a negligible gravitational gradient, the pressure gauge or transducer can be located outside the vessel.

The rock sample is usually machined into a cylindrical shape. In order to prevent the pressurizing fluid from entering the pore space of the rock, the specimen

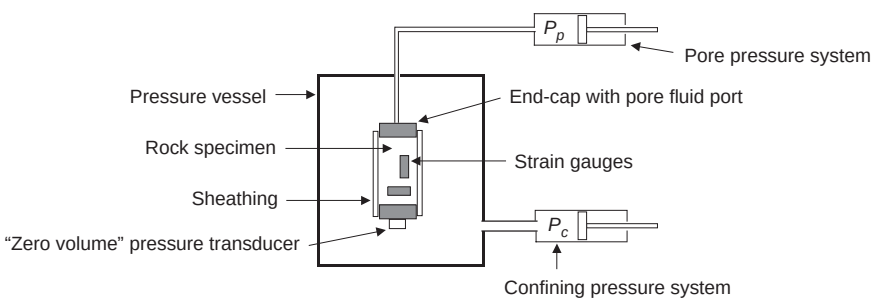

Fig. 6.1 Schematic diagram of typical experimental system used to measure compression of a porous rock subjected to hydrostatic confining pressure and pore pressure (after Hart and Wang, 2001).

must be covered with a tight-fitting, impermeable sheathing, such as heat-shrink tubing. The volumetric strain of the specimen can be measured by strain gauges glued onto the sides. If the rock is isotropic, the radial, circumferential, and axial strains should all be equal. Nevertheless, it is advisable to measure the strains in more than one direction.

If the rock is porous and permeable, a variable pore pressure can also be applied to the specimen. Furthermore, other poroelastic parameters, described in §7.2, can be measured under these hydrostatic conditions. In a typical configuration (Fig. 6.1), the two flat faces of the cylindrical specimen are fitted with metal end-caps, which have small holes drilled into them, through which the pore fluid can flow. The pore fluid is collected outside the pressure vessel in a piston-like device that allows the pore fluid pressure, and the extruded volume of the pore fluid, to be controlled and monitored. Such experimental configurations are described in more detail by Zimmerman et al. (1986), Hart and Wang (2001), and Lockner and Stanchits (2002).

As discussed in §7.2, a poroelastic rock has four fundamental compressibilities, which relate changes in the hydrostatic confining stress and pore pressure to the resulting pore or bulk strains. The bulk compressibility C_{bc} can be found by measuring the bulk strain that occurs in response to a change in confining pressure, with the pore pressure held constant. The other bulk compressibility, C_{bp}, is found from the bulk strain that occurs when the pore pressure is changed and the confining pressure is held constant. These two measurements pose no major difficulties.

The pore compressibility C_{pc} quantifies the pore strain that results from changing the confining pressure, with the pore pressure held constant. If the pore pressure is constant, then the volume of pore fluid in the system is constant, and so the change in the pore volume of the rock is exactly equal to the volume of pore fluid that enters or leaves the pore pressure piston device. Hence, measurement of C_{pc} poses no fundamental difficulty.

Measurement of the other pore compressibility, C_{pp}, which quantifies the change in pore volume caused by a change in pore pressure, with the confining pressure held constant, is not so straightforward. As the pore fluid is varied, the total volume of pore fluid will change, through the relation $\Delta V_f = -C_f V_f \Delta P_p$, where C_f is the compressibility of the pore fluid. Some of this volume change will occur in the pore space of the rock, some will occur in the tubing leading from the specimen to the pore pressure piston, and some will occur within the piston itself. Specifically,

$$\Delta V_{\text{fluid}} = \Delta V_{\text{pore}} + \Delta V_{\text{tubing}} + \Delta V_{\text{piston}}. \tag{6.1}$$

The term ΔV_{piston} is measured directly, whereas the desired quantity is ΔV_{pore}. Estimation of the actual pore volume change therefore requires knowledge of the other two terms in (6.1). This can in principle be achieved by first performing calibration tests, for example using an effectively rigid specimen such as one made of steel, to determine the compliance of the tubing and the total storativity, $C_f V_f$, of the pore fluid. However, the two unwanted terms in (6.1) are generally at least

as large as the change in pore volume, rendering the estimation of the pore volume change quite problematic (Hart and Wang, 1995).

Another related "hydrostatic" elastic parameter of a porous rock is Skempton's B coefficient (Skempton, 1954). This parameter is defined, in (7.28), as the ratio of the pore pressure increment to the confining pressure increment, when the confining pressure is varied under "undrained" conditions, in which no fluid is permitted to leave the specimen. However, in a configuration such as that of Fig. 6.1, some pore fluid must indeed leave the specimen in order to enter the piston device. If the piston is replaced by a pressure transducer, it is nevertheless true that the pressure response of the pore fluid is influenced by both the compliance of the pore space of the specimen and by the compliance of the tubing and transducer. These effects can again in principle be accounted for by proper calibration, but in practice, this is quite difficult to achieve accurately, as the system compliance may be of the same magnitude as that of the pore space. Accurate measurements of B can presumably be obtained by placing a "zero volume" pressure transducer in immediate contact with the specimen, inside the pressure vessel (Hart and Wang, 2001), thus eliminating the effects of system compliance.

6.3 Uniaxial compression

The uniaxial compression test, in which a right circular cylinder or prism of rock is compressed between two parallel rigid plates (Fig. 6.1), is the oldest and simplest mechanical rock test and continues to be widely used. This test is used to determine the Young's modulus, E, and also the unconfined compressive strength, C_o.

In the simplest version of this test, Fig. 6.2a, a cylindrical core is compressed between two parallel metal platens. Hydraulic fluid pressure is typically used to apply the load. The intention of this test is to induce a state of *uniaxial stress* in the specimen, that is,

$$\tau_{zz} = \sigma, \quad \tau_{xx} = \tau_{yy} = \tau_{xy} = \tau_{yz} = \tau_{xz} = 0. \tag{6.2}$$

The axial stress σ is the controlled, independent variable, and the axial strain is the dependent variable. The longitudinal strain can be measured by a strain gauge glued to the lateral surface of the rock. Alternatively, the total shortening of the core in the direction of loading can be measured by an extensiometer that

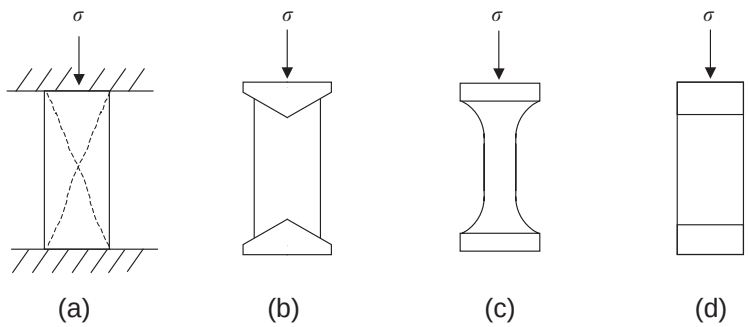

Fig. 6.2 Unconfined uniaxial compression of a rock: (a) standard configuration, with failure initiating at the corners, (b) conical end-pieces to eliminate frictional restraint, (c) tapered specimen, (d) matched end-pieces.

monitors the change in the vertical distance between the platens. In this case, the longitudinal strain is calculated from the relative shortening of the core, that is, $\varepsilon = -\Delta L/L$. If the stress state were indeed uniaxial, then the Young's modulus of the rock could be estimated from $E = \sigma/\varepsilon$. The stress can be increased slowly until failure occurs, as discussed in §4.2. The stress at which the rock fails is known as the *unconfined*, or *uniaxial*, compressive strength of the rock.

Unfortunately, the actual state of stress in the rock core, in a configuration such as that of Fig. 6.2a, will not be a homogeneous state of uniaxial compression. This is due primarily to the constraining influence of the frictional forces acting along the interface between the core and the platens. A true uniaxial stress state would lead to lateral expansion associated with the Poisson effect, (5.12). But this lateral expansion is hindered at the platens due to friction. A more realistic boundary condition to assume for the rock core is that of uniform vertical displacement and no lateral displacement (Filon, 1902; Pickett, 1944; Edelman, 1949). Hence, in a testing configuration such as shown in Fig, 6.2a, the rock core would bulge outward away from the end platens, but would be constrained against such bulging at the platens, thereby taking on a barrel-shape.

This lack of homogeneity in the stress state has implications both for the measurement of the elastic modulus and the compressive strength. Although the stress state indeed approaches that of uniaxial stress away from the platens, in the middle of the core, it is much more complex and inhomogeneous at the ends. Hence, it is not obvious that $-\sigma L/\Delta L$ will yield a correct estimate of E. Chau (1997) presented an accurate approximate solution to this problem, for the case in which the friction between the end platens and the rock is sufficiently large that no lateral motion of the rock can occur at the two boundaries. He expressed his results in terms of a parameter λ, defined as the ratio of the "true" Young's modulus to the "apparent" value estimated from $E = -\sigma L/\Delta L$. As would be expected, this factor approaches unity as the Poisson ratio goes to zero, since in this case the tendency for lateral expansion does not arise. For cores in which the length is at least as large as the diameter, and for which the Poisson ratio is less than 0.3 (which will usually be the case), the factor λ was found to lie in the range 0.97–1.0. Greenberg and Truell (1948) carried out a similar analysis for a rectangular prism compressed in plane strain conditions, with a Poisson ratio of 0.33, and found $\lambda = 0.96$. Hence, as far as the calculation of E is concerned, the issue of friction along the rock/platen interface is probably not of engineering significance.

Nevertheless, this frictional restraint leads to a stress concentration at the corners of the rock core, at the points where it meets the platen. This causes a shear fracture to initiate at that point, as shown in Fig. 6.2a, at an applied (nominal) stress σ that is actually less than the "true" uniaxial compressive strength. Several methods have been proposed to avoid this problem. One suggested approach is to machine the specimens to have hollow conical ends and then to compress them between conical end-pieces, the surfaces of which are inclined to the diameter of the specimen at the angle of friction (Fig. 6.2b).

Barnard (1964), Murrell (1965) and others have used shaped specimens that have a smaller diameter in the necked midregion than near the ends (Fig. 6.2c).

The shape of the specimen is carefully chosen, based on photoelasticity studies or finite element analysis, so that the stress distribution is uniform across the section in the neck. This permits the true Young's modulus to be calculated from the longitudinal strains measured in the neck with strain gauges, and also avoids the problem of shear fractures initiating at the point of the stress concentration near the platens. These shaped specimens are difficult to prepare, however, and tend by necessity to have short necked regions.

Another approach to mitigating the problems of stress concentrations at the platens is to compress the rock core between metal end-pieces that have the same diameter as the core and are made of a metal that has the same ratio of ν/E as does the rock (Fig. 6.2d). In this case, the lateral expansion of the rock at its ends should match that of the platens, eliminating the unwanted stress concentrations. This approach has been used by Cook (1962) and others.

Labuz and Bridell (1993) carried out compression tests on granite cores, with various lubricants applied between the core and the platens. Radial strains were measured near the ends and in the central portion of the core, to investigate the barreling effect. In the absence of lubrication, the radial hoop strains were as much as 50 percent higher in the central region of the core than near the ends. By testing various lubricants, including graphite and molybdenum disulfide, they found that this stress inhomogeneity could essentially be eliminated by the application of a mixture of stearic acid and petroleum jelly to the rock-platen interface.

6.4 Triaxial tests

One of the most widely used and versatile rock mechanics tests is the traditional "triaxial" compression test. Indeed, much of the current understanding of rock behavior has come from such tests. Despite the name, which would seem to imply a state of three independent principal stresses, in a triaxial test, a rock specimen is subjected to a homogeneous state of stress in which two of the principal stresses are of equal magnitude. Typically, all three stresses are compressive, with the unequal stress more compressive than the two equal stresses, so that $\sigma_1 > \sigma_2 = \sigma_3 > 0$.

The restriction of traditional triaxial tests to stress states in which two of these stresses are necessarily equal in magnitude is imposed by experimental limitations. Consequently, despite the ubiquitous nature of triaxial tests and triaxial compression data on rocks, it should not be erroneously concluded that stress states in which two principal stresses are of equal magnitude are particularly common in the subsurface. Indeed, there is no particular reason for σ_2 and σ_3 to be equal, either in undisturbed rock or in the vicinity of an excavation.

A triaxial stress state can be achieved by subjecting a cylindrical rock specimen to uniaxial compression by a piston, as described in §6.3, in the presence of hydrostatic compression applied by a pressurized fluid, as described in §6.2. Depending on the experimental configuration, the hydrostatic pressure may act in all three directions or only over the two lateral surfaces of the rock. In either case, the value of the two equal lateral stresses, $\sigma_2 = \sigma_3$, is known in this context as the *confining stress* and the other principal stress is referred to as the *axial*

stress. The difference between the axial stress and the confining stress, $\sigma_1 - \sigma_3$, is referred to as the *differential stress*.

The classic triaxial compression tests on a rock were those performed by von Kármán (1911) on specimens of Carrara marble, using an apparatus that can be said to have served since as the prototype for triaxial testing machines. His machine and procedure, along with subsequent improvements, are described in detail by Paterson (1978, Chapter 2), upon which some of the following discussions are based.

Triaxial tests are usually conducted with cylindrical specimens having a length-to-diameter ratio of between 2:1 and 3:1. It is imperative that the flat surfaces of the specimen be as nearly parallel as possible, to avoid bending of the specimen under the axial stress. The core is jacketed in rubber or thin copper tubing so that the confining fluid does not penetrate into the pore space (Fig. 6.3a). If the effect of pore pressure is to be investigated, pore fluid would be introduced into the rock through a small hole in one of the end-pieces, as described in §6.2.

A simple triaxial apparatus is the one developed at the US Bureau of Reclamation (Fig. 6.3b). A spherical seat is used on one end-piece to correct for the possibility that the platens are not parallel. However, this apparatus has two disadvantages. Firstly, the confining pressure acts against the loading piston, so that the applied axial force must be large enough to overcome this force, in addition to creating the axial stress. Secondly, as the specimen compresses, the volume of the confining fluid in the cell decreases, making it difficult to control the confining pressure. This effect can be greatly diminished by having the pistons and end-pieces be of the same diameter as the specimen and by minimizing the volume available to the confining fluid (Donath, 1966).

Griggs et al. (1960) and Paterson (1964) avoid interaction between the axial displacement of the end-pieces and the confining pressure completely, by using two pistons connected by a yoke, only one of which applies load to the specimen. This arrangement allows the volume of confining fluid to remain constant as the axial load is increased. It also allows the confining fluid pressure to act in the axial direction, not only in the lateral directions, so that the loading piston needs only

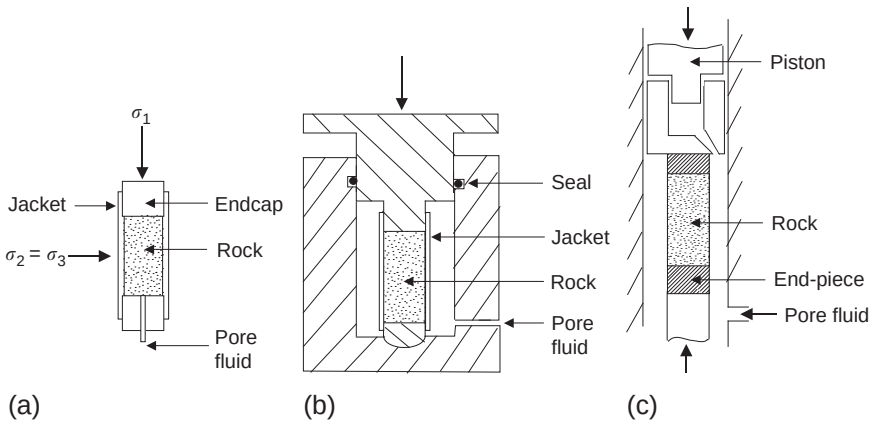

Fig. 6.3 Triaxial testing apparatus: (a) jacketed cylindrical rock specimen with end-pieces and provision for pore fluid, (b) US Bureau of Reclamation cell, (c) central portion of a constant-volume triaxial cell.

to supply enough force to create the differential load and to overcome friction, but does not need to overcome the confining pressure (Fig. 6.3c).

The variables that must be measured in a triaxial test include the confining stress, the axial stress (or the differential stress), the axial strain, and the lateral strain. The confining stress acting on the rock is easily measured by measuring the pressure of the confining fluid with a pressure gauge or an electronic pressure transducer, which may for convenience be placed outside the cell. The axial stress can be calculated from the pressure of the oil in the loading jack, after correcting for the area ratio, although such a calculation ignores friction along the sides of the piston. Alternatively, the axial load can be measured by placing in series with the rock specimen a *load cell*, which is essentially a metal element of known elastic modulus to which strain gauges are attached (Davis and Gordon, 1968). The axial (ε_{zz}) and lateral ($\varepsilon_{\theta\theta}$) normal strains of the rock are most accurately measured by strain gauges glued to the outer face of the cylindrical rock core. To avoid end effects, these gauges are usually placed midway between the two end-pieces.

If the axial stress is smaller in magnitude than the two lateral stresses, but nevertheless still compressive, the resulting state of stress, $\sigma_1 = \sigma_2 > \sigma_3 > 0$, is referred to as *triaxial extension* (Heard, 1960). Such tests are useful in testing Mohr's assumption that failure is not influenced by the magnitude of the intermediate principal stress. Triaxial extension tests are readily conducted in a triaxial testing apparatus, provided that the piston can be suitably attached to the end-pieces.

6.5 Stability and stiff testing machines

As discussed in §4.2, many rocks exhibit a postpeak, strain-softening regime in which the tangent modulus, $E_{\text{tan}} = \mathrm{d}\sigma/\mathrm{d}\varepsilon$, is *negative*. This does not conform to one of the basic assumptions of the theory of elasticity, which is that the elastic modulus should be positive in order for the stored strain energy function to be positive-definite; see §5.8. Although positivity of E is not required by any thermodynamic law, a negative tangent modulus can, under certain situations, give rise to unstable behavior. This has important implications during laboratory compression tests.

To understand the inherent instability of a rock having a negative tangent modulus, consider a cylindrical rock specimen of length L and cross-sectional area A, compressed under a weight, W, as in Fig. 6.4a. The stress–strain behavior of the rock will be represented in the idealized form of Fig. 6.4b, in which a linear elastic regime with modulus E is followed by a strain-softening regime with modulus $E_{\text{tan}} = -|E_{ss}|$, where this notation is used to underscore the fact that the tangent modulus is negative in this regime.

Imagine that the load W is precisely large enough so that the rock is loaded to its elastic limit, denoted by point B in Fig. 6.4b. At this point, the stress in the rock is $\sigma = W/A$, the strain is $\varepsilon = W/AE$, and the stored strain energy is $\mathcal{E} = W^2L/2AE$. Now imagine that the rock somehow compresses by an additional amount Δz, without the introduction of any additional energy into the system, so that it moves to point C on the stress–strain curve. The change in

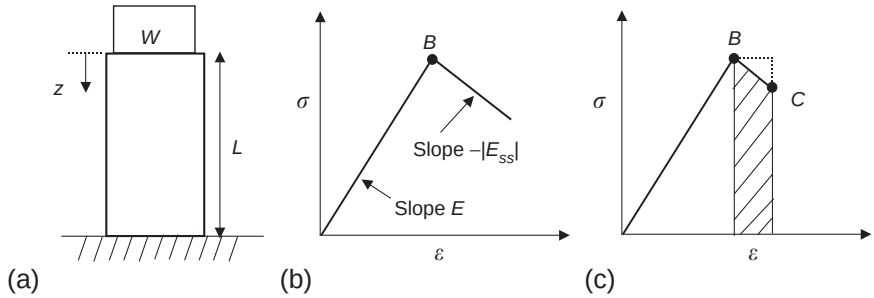

Fig. 6.4 (a) Rock cylinder loaded by a weight, W; (b) idealized stress–strain curve of a rock exhibiting strain-softening behavior; (c) work done on rock by additional compression from B to C.

the total energy of the system must be zero, that is,

$$\Delta \mathcal{E} = \Delta \mathcal{E}_{\text{elastic}} + \Delta \mathcal{E}_{\text{gravitational}} + \Delta \mathcal{E}_{\text{other}} = 0, \tag{6.3}$$

where $\mathcal{E}_{\text{other}}$ represents energy that may be available to cause additional damage to the rock in the form of microcracking, etc. The gravitational potential energy of the load decreases by $W\Delta z$, so $\Delta \mathcal{E}_{\text{grav}} = -WL\Delta\varepsilon$. The strain energy stored in the rock, per unit volume, *increases* by an amount equal to the shaded area in Fig. 6.4c. This area is equal to the area of the rectangle of height σ and width $\Delta\varepsilon$, *minus* the area of the small triangle having base $\Delta\varepsilon$ and height $|E_{ss}|\Delta\varepsilon$. After multiplying by the volume of the rock,

$$\Delta \mathcal{E}_{\text{elastic}} = AL[\sigma\,\Delta\varepsilon - \frac{1}{2}|E_{ss}|\Delta\varepsilon^2] = WL\,\Delta\varepsilon - \frac{AL}{2}|E_{ss}|\Delta\varepsilon^2. \tag{6.4}$$

From (6.3), the change in the "other" energy that is available to further degrade the rock will be

$$\begin{aligned}\Delta \mathcal{E}_{\text{other}} &= -\Delta \mathcal{E}_{\text{elastic}} - \Delta \mathcal{E}_{\text{grav}} \\ &= -WL\Delta\varepsilon + \frac{AL}{2}|E_{ss}|\Delta\varepsilon^2 - (-WL\Delta\varepsilon) = \frac{AL}{2}|E_{ss}|\Delta\varepsilon^2 > 0.\end{aligned} \tag{6.5}$$

Hence, a small additional compression of the rock will liberate a positive amount of energy, which will be available to cause further microscale degradation of the rock, thereby causing further softening of the tangent modulus, etc. It is clear that this is an unstable process that will inevitably lead to complete disintegration of the specimen.

If the tangent modulus were positive at point B, the quadratic term in (6.4) would be positive, and (6.5) would show the energy available for cracking the rock to be negative, which by definition is not possible. In this case, the additional compression of the rock would *not* spontaneously occur without the addition of external energy to the system (such as by increasing the load, W). Hence, a negative tangent modulus is necessary for this type of instability to occur.

Having established that a negative value of the tangent modulus may lead to instabilities under certain experimental conditions, we now consider a more realistic model for a traditional rock-testing machine, as used in uniaxial compression tests, by considering the effect of the compliance of the machine (Salamon, 1970; Hudson et al., 1972; Hudson and Harrison, 1997, pp. 89–92). Consider a

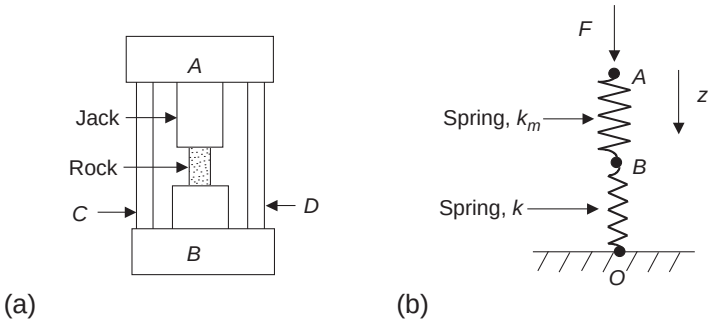

Fig. 6.5 (a) Simplified model of a testing machine used to compress a rock. (b) Idealization in which the machine stiffness is represented by a spring k_m and the rock is represented by a (nonlinear) spring, k.

rock-testing apparatus such as shown in Fig. 6.5a. As the rock specimen is compressed by the hydraulic jack, the jack exerts a downward force F on the rock, and, according to Newton's third law, the rock exerts an upward force F on the jack. As the load F increases, additional elastic energy is of course stored in the rock, but it is also stored in the hydraulic system, the platens, the vertical bars C and D, and other parts of the apparatus. For conceptual simplicity, the entire loading system can be represented by an elastic spring of stiffness k_m, defined such that if the load is F, the energy stored in the loading system is $F^2/2k_m$. The rock specimen can also be thought of as a spring, with stiffness $k = EA/L$. At equilibrium, the two springs are subjected to the same force, F, so they can be assumed to be in series (Fig. 6.5b).

Assume again that the system is in equilibrium, with the rock compressed to point B in Fig. 6.4c. In this state, the compressive force in both springs is F. Now imagine that the rock spontaneously undergoes an additional small compression, moving to point C on its stress–strain curve. With respect to the spring model in Fig. 6.5b, point B is displaced downward by an amount Δz_B. If this occurs without the addition of any energy to the system, this is equivalent to specifying that no displacement can occur at point A in Fig. 6.5b. By definition, no displacement occurs at point O.

Following the same argument as was used to derive (6.4), but replacing the load W with F, and noting that $\Delta\varepsilon = \Delta z/L$, the change in the amount of strain energy stored in the rock specimen is

$$\Delta\mathcal{E}_{\text{specimen}} = F\Delta z_B - \frac{1}{2}\frac{A|E_{ss}|}{L}(\Delta z_B)^2. \tag{6.6}$$

For a small displacement Δz_B, this term is clearly positive, reflecting the fact that the rock continues to absorb energy, even as it deforms into its strain-softening regime. A similar argument for the elastic energy stored in the testing machine gives

$$\Delta\mathcal{E}_{\text{machine}} = -F\Delta z_B + \tfrac{1}{2}k_m(\Delta z_B)^2. \tag{6.7}$$

The energy stored in the testing machine decreases, as the machine is undergoing *unloading* in this regime. This can be seen from Fig. 6.5b, where a downward displacement of point B will *decrease* the amount of compression in the spring representing the testing machine. Hence, the amount of additional energy that

is liberated, and is therefore available to cause further degradation of the rock, is

$$\Delta \mathcal{E}_{\text{other}} = -\Delta \mathcal{E}_{\text{specimen}} - \Delta \mathcal{E}_{\text{machine}} = \frac{1}{2}\left[\frac{A|E_{ss}|}{L} - k_m\right](\Delta z_B)^2. \tag{6.8}$$

If this term is positive, the system will be unstable, as this energy will cause further microcracking of the rock, etc. Hence, the condition for *stability* is that the stiffness of the testing machine, k_m, be *greater* than $A|E_{ss}|/L$, where A is the cross-sectional area of the specimen, L is its length, and E_{ss} is the slope of the stress–strain curve of the rock in the strain-softening regime. A testing machine is categorized as being *stiff* or *soft*, with respect to a given rock specimen, depending on whether or not it satisfies this criterion.

The condition for the onset of instability of this system can also be derived by the following simple argument (Salamon, 1970). At equilibrium, the compressive forces in the two springs in Fig. 6.5b are equal, so $k_m(z_A - z_B) = k(z_B - z_O) = kz_B$, where the displacements of each of the three points (A, B, O) are measured starting from their values at $F = 0$. Let the force F be increased slightly by ΔF. If we require that the system move to a new equilibrium state, then the displacements must satisfy the constraint of force equilibrium, and so $k_m(\Delta z_A - \Delta z_B) = k\Delta z_B$. In general, $k = E_{\tan}A/L$, and so, since $\Delta z_B = L\Delta\varepsilon$, this relation can be solved to give

$$\Delta\varepsilon = \frac{k_m}{Lk_m + AE_{\tan}}\Delta z_A. \tag{6.9}$$

In the elastic regime of the rock's behavior, $E_{\tan}$ will be positive, and (6.9) can be solved to uniquely determine the additional incremental strain in the rock. However, if the rock softens sufficiently that $E_{\tan} = -Lk_m/A$, there will be no finite solution to (6.9), implying that the rock cannot deform to a new equilibrium state – it will fail catastrophically. As was the case for the derivation based on energy considerations, the condition for stability is $k_m > A|E_{\tan}|/L$.

In reality, the transition from a positive tangent modulus to a negative tangent modulus occurs gradually, not abruptly as in Fig. 6.4b. If a rock is compressed in a "soft" machine, unstable disintegration of the rock will commence when the slope of the stress–strain curve first becomes sufficiently negative that $|E_{\tan}|$ equals Lk_m/A. This will typically occur at a point very near the peak of the stress–strain curve; the rock will fail abruptly and explosively, and it will not be possible to observe and measure the strain-softening portion of the stress–strain curve. An understanding of the role of machine compliance in obscuring the softening portion of the stress–strain curve was first developed by Whitney (1943) and others in the context of concrete testing, but was not fully appreciated in the field of rock mechanics until the 1960s (Hudson et al., 1972).

There are many sources of elastic compliance in a testing machine, such as the hydraulic system, the vertical columns (C and D in Fig. 6.5a), the crossheads (A and B), etc. As each of these are subject to the same load, the compliances are additive. The individual stiffnesses k_i are therefore combined by adding their reciprocals, so that $k_m = [\Sigma(1/k_i)]^{-1}$. One approach to solve this instability problem is to minimize the individual sources of elastic compliance in the system.

The largest contributions to the compliance typically come from the hydraulic system and the columns (Cook and Hojem, 1966). Cook and Hojem constructed a machine with a stiff frame and minimized the compliance of the hydraulic system by using for the hydraulic system a short column of mercury with a large cross-sectional area. This apparatus was used by Crouch (1970,1972) to study the compressional behavior of quartzite and norite.

A quite different approach to stiffening a testing machine is to add a stiff element in *parallel* with the rock specimen, so that the stiffener and the specimen undergo the same displacement. In this case the overall stiffness will be the sum of that of the machine and that of the stiffener. Cook (1965) stiffened a conventional testing machine by loading a steel ring in parallel with the rock specimen and was able to significantly reduce the explosive nature of the failure of a specimen of Tennessee marble. Bieniawski et al. (1969) used a similar apparatus to study the compression of sandstone and norite.

A third approach is to use the thermal expansion/contraction of the columns in the testing machine to supply the force needed to compress the rock. Cook and Hojem (1966) constructed a testing machine in which a hydraulic jack was used to prestress the specimen and the remaining displacement was induced by thermal contraction of the vertical columns.

Each of the proposed solutions to the machine stiffness problem has serious drawbacks, however. There are practical limits to the extent to which one can eliminate sources of compliance within a testing machine. Adding a stiffening element in parallel has the unwanted effect of decreasing the effective load capacity of the system, as much of this capacity will be used to compress the stiffening member. Finally, it is very difficult to control the rate at which the load is applied when thermal contraction of the columns is used to compress the rock.

The unstable collapse and disintegration of the specimen are caused by the rapid flow into the specimen of some of the energy that had been stored in the machine. Much of this energy is stored in the hydraulic system. If, for example, fluid could be drawn out of the hydraulic system rapidly and in a controlled manner, this problem could be avoided. This can indeed be achieved with servo-controlled testing machines (Bernhard, 1940; Rummel and Fairhurst, 1970). A main idea behind the performance of these machines is that, to trace out the full stress–strain curve beyond the point of peak strength, the strain in the rock specimen must be the controlled variable. With regards to the loading platens, this implies that the displacement, rather than the load, is the variable that must be controlled. In a servo-controlled testing machine, the deformation of the rock is monitored and then compared to the desired strain. Any difference between the desired and current strain is used to create a "correction signal" that adjusts the hydraulic pressure so as to bring the actual strain closer to the desired value; see Hudson et al. (1972) and Hudson and Harrison (1997) for details. The response time of such systems is in the order of a few milliseconds, which is sufficiently rapid to be able to arrest the unstable disintegration of the rock (Rummel and Fairhurst, 1970). Thus, the full stress–strain curve can be obtained, provided that the strain increases monotonically.

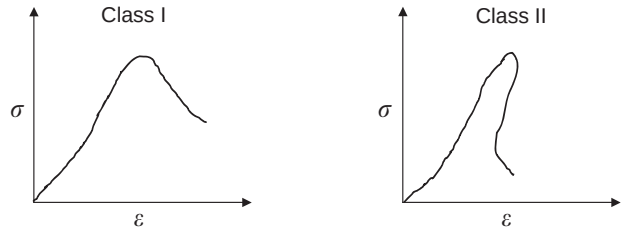

Fig. 6.6 Class I and Class II stress–strain curves.

Some rocks, however, exhibit a complete stress–strain curve in which neither the stress nor the strain increases monotonically. For such rocks, denoted by Wawersik and Fairhurst (1970) as "Class II," the stress and strain each decreases as the rock begins to fail (Fig. 6.6). This occurs as the rock continues to deteriorate on a microscopic scale and is fundamentally different from elastic unloading with hysteresis. Okubo and Nishimatsu (1985) showed that by using a linear combination of stress and strain as the feedback signal in a servo-controlled testing machine, the complete stress–strain curves of both Class I and Class II rocks can be obtained.

6.6 True-triaxial tests

Traditional "triaxial" compression tests, such as described in §6.4, involve states of stress in which $\sigma_1 > \sigma_2 = \sigma_3 > 0$. Such tests are incapable of probing the effects of the intermediate principal stress. In order to investigate rock behavior over the full range of stresses that may occur in the subsurface, it would be desirable to conduct tests in which all three principal stresses may have different (compressive) values. Such tests have sometimes been referred to as "polyaxial," although this name has the disadvantage of not being self-explanatory. More recently, the term "true-triaxial," which is inelegant but less open to misinterpretation, has gained acceptance.

Several researchers have constructed testing cells that attempt to produce states of homogeneous stress in which the three principal stresses, $\sigma_1 \geq \sigma_2 \geq \sigma_3 \geq 0$, are independently controllable (Fig. 6.7a). Although the designs differ in various ways, in each case a "rectangular" (i.e., parallelepiped-shaped) specimen is used, in contrast to the cylindrical specimens used in traditional triaxial tests. Hojem and Cook (1968) constructed a cell in which the two lateral stresses σ_2 and σ_3 were applied to the specimen by two pairs of thin copper flat jacks and the axial load was applied by a traditional loading piston. However, it was difficult to apply high lateral stresses with this apparatus, thus limiting its range of usefulness.

Mogi (1971) built an apparatus in which the minimum stress, σ_3, was applied by a pressurized fluid, and the two other stresses were applied by opposing sets of flat jacks (Fig. 6.7b,c). The choice of having the minimum stress applied by fluid pressure was made so that this stress could be measured with the greatest accuracy. The specimen was in the form of a rectangular prism, 1.5 cm × 1.5 cm in cross section and 3.0 cm long in the σ_1 direction. The steel end-pieces over which σ_1 was applied were connected to the specimen by epoxy, whereas the end-pieces over which σ_2 was applied were coupled to the specimen through thin rubber lubricating sheets. The sides of the specimen were jacketed with

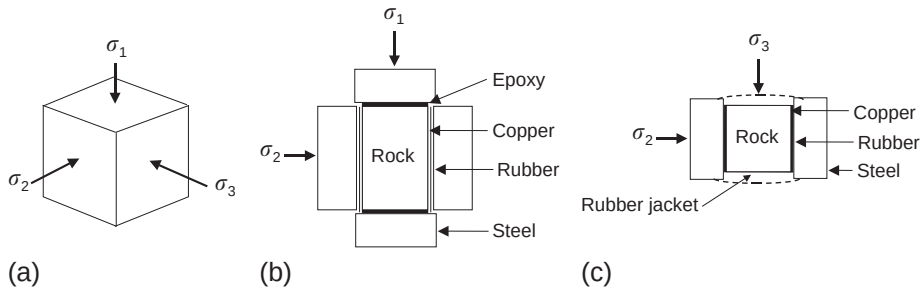

Fig. 6.7 (a) True-triaxial state of stress applied to a cubical specimen; (b) view along the σ_3 direction of the apparatus used by Mogi (1971); (c) view along the σ_1 direction.

thin copper sheets to prevent the rubber from intruding into the rock, and a silicon rubber jacket was used to prevent the pressurizing fluid from entering the pores of the rock. Mogi used this apparatus to investigate the influence of the intermediate principal stress on the yield and fracture of several rock types.

Haimson and Chang (2000) built a compact and portable true-triaxial cell based on Mogi's design. Their apparatus can subject a specimen to values of σ_1 and σ_2 as high as 1600 MPa and σ_3 as high as 400 MPa. Normal strains in the direction of maximum and intermediate stress were measured with strain gauges glued to the respective faces of the specimen, whereas the third strain was measured with a beryllium-copper beam fitted with a strain gauge. The center of the beam makes contact with a pin affixed to the face of the specimen, and as the rock expands in the σ_3 direction, the beam bends outward, and its deflection is measured by the strain gauge. This apparatus was used to investigate the influence of the intermediate stress on the failure of Westerly granite, which was found to be significant. No such effect of σ_2 was found for a hornfels and a metapelite from the Long Valley caldera in California (Chang and Haimson, 2005).

Hunsche and Albrecht (1990) describe an apparatus that uses three pairs of double-acting pistons to apply three independently variable normal stresses to the faces of a cubical specimen. Heaters placed between the specimen and the pistons allowed the rock to be heated to 400°C. The forces applied by each pair of pistons were calculated from pressure gauges in the hydraulic lines. Deformation of the specimen in the three directions was measured with linear variable displacement transducers (LVDTs), which essentially measure the change in the distance between the opposing platens. Paraffin wax (at room temperature) and graphite (at elevated temperatures) were used as lubricants between the platens and rock. This apparatus was used to study the deformation of rock salt, and it was found that the observed strength of the rock, defined as the maximum value of the octahedral shear stress, depended sensitively on the ratio of specimen size to platen size. Sayers et al. (1990) describe a similar apparatus that is fitted with ultrasonic transducers in each end-piece, so as to be able to measure shear and compressional wavespeeds under states of true-triaxial stress.

6.7 Diametral compression of cylinders

The difficulties associated with performing a direct uniaxial tension test on rock have led to the development of a number of "indirect" methods for assessing the tensile strength. Such methods are called indirect because they do not involve

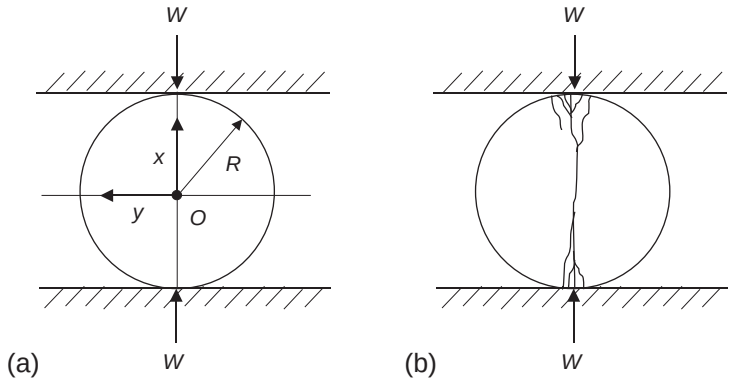

Fig. 6.8 (a) Cylinder compressed between parallel surfaces by a line load W (per unit length into page); (b) typical fracture pattern resulting from this loading.

the creation of a homogeneous state of tensile stress in rock, but rather involve experimental configurations that lead to inhomogeneous stresses that are tensile in some regions of the specimen. The precise value of the tensile stress at the location where failure initiates must be found by solving the equations of elasticity.

The most popular of these tests is the so-called *Brazilian test*, developed by the Brazilian engineer Fernando Carneiro in 1943 for use in testing concrete. A thin circular disk of rock is compressed between two parallel platens, so that the load is directed along the diameter of the disk (Fig. 6.8a). As the platens are relatively rigid compared to the rock, they can be assumed to apply a point load W (per axial length of the cylinder) to the two opposing loading points. With the coordinate system taken as in Fig. 6.8a, the stresses along this vertical diameter are, by (8.165),

$$\tau_{xx} = \frac{-W}{\pi R}, \quad \tau_{yy} = \frac{W(3R^2 + x^2)}{\pi R(R^2 - x^2)}, \tag{6.10}$$

whereas along the y-axis, perpendicular to the load, the stresses are

$$\tau_{xx} = \frac{-W(R^2 - y^2)^2}{\pi R(R^2 + y^2)^2}, \quad \tau_{yy} = \frac{W(R^2 - y^2)(3R^2 + y^2)}{\pi R(R^2 + y^2)^2}. \tag{6.11}$$

By symmetry, these stresses are principal stresses. The largest and smallest principal stresses occur on the vertical axis, through which the load passes. The minimum principal stress, τ_{xx} in (6.10), is uniform and *tensile* along this entire axis. The maximum principal stress, τ_{yy} in (6.10), is compressive and becomes unbounded near the platens, but varies only weakly near the center of the disk. At the center of the disk, the two principal stresses are, by setting $x = 0$ in (6.10),

$$\tau_{xx} = \frac{-W}{\pi R}, \quad \tau_{yy} = \frac{3W}{\pi R}. \tag{6.12}$$

As the disk is in a state of plane stress, the third principal stress, normal to the plane of the disk, is zero, and consequently is the intermediate principal stress.

When a cylindrical rock specimen is compressed in this way, failure typically occurs by an extension fracture in, or close to, the loaded diametral plane, at

some value of the applied load W, as in Fig. 6.8b. It is generally assumed that the failure is the result of the tensile stress $\tau_{xx} = \tau_{\theta\theta} = -W/\pi R$, and so the tensile strength is given by the value of $W/\pi R$ at failure. Tensile strengths measured in this way are very reproducible and are in reasonable agreement with values obtained in uniaxial tension. The Brazilian indirect tension test has been used to determine the tensile strength of coal by Berenbaum and Brodie (1959), and of various sandstones and siltstones by Hobbs (1964).

If the applied load is actually a uniform normal stress of magnitude σ, distributed over a small arc of angle 2α, then the state of stress near the points of contact will be a uniform compression of magnitude σ. This will decrease the likelihood of failure by shear fracture at the contact points, but has virtually no effect on the stresses near the center of the disk. Hence, Brazilian tests conducted with loads distributed over a narrow arc, such as 15°, yield values of the tensile strength that are little different from those obtained using line loads and give rise to similar diametral extension fractures.

If jacketed cylinders are subjected to confining pressure p applied by a pressurized fluid, as well as to diametral compression, then at the center of the disk a hydrostatic stress p would be added to the three principal stresses discussed above, leading to

$$\sigma_1 = (3W/\pi R) + p, \quad \sigma_2 = p, \quad \sigma_3 = p - (W/\pi R). \tag{6.13}$$

This configuration gives a means of studying failure in situations where all three stresses are compressive, but σ_3 is small, as is often the case near an underground excavation. The three principal stresses will be connected by the relation

$$\sigma_1 - 4\sigma_2 + 3\sigma_3 = 0, \tag{6.14}$$

so this test will determine a curve defined by the intersection of the failure surface with the surface defined by (6.14). Jaeger and Hoskins (1966a) found that the values of σ_1 and σ_3 obtained from these tests, using (6.13), agreed reasonably well with those obtained in standard triaxial compression tests, although the values of σ_1 tended to be consistently higher than those measured in the triaxial tests for the same value of σ_3. They attributed this to the strengthening effect of the intermediate principal stress, as discussed in §4.8.

The analysis presented above assumes that the rock is isotropic, which may not be the case. Chen et al. (1998) developed a mathematical solution for the diametral compression of a thin disk of rock that is transversely isotropic in the plane of the disk. In this case, the analysis of the results is complicated by the fact that the two principal stresses at the center of the disk depend, in a complicated and implicit manner, on the values of the elastic moduli. Claesson and Bohloli (2002) analyzed this solution further and derived accurate approximate expressions for these stresses. Lavrov and Vervoort (2002) presented a solution that accounts for the influence of transverse tractions applied at the rock–platen interface, caused by friction, and showed that such tractions would have little effect on the stresses at the center of the disk and hence little effect on the interpretation of tests in which failure initiated at or near the center.

6.8 Torsion of circular cylinders

As discussed in §6.3, Young's modulus, E, can be measured by subjecting the rock to a state of homogeneous uniaxial compression. The shear modulus, G, could in principle be measured by inducing a state of homogeneous *shear* stress in a rock specimen. The shear modulus would be found from the ratio of the shear stress to the shear strain. However, it is not easy to induce a homogeneous state of shear in a piece of rock. But an inhomogeneous state of shear can be induced in a circular cylinder by subjecting it to torsion. Analytical solution of the elasticity equations for this configuration yields a simple relationship between the applied torque, the angle of twist, and the shear modulus. Hence, measurement of the applied torque and the resulting angle of twist will permit G to be calculated.

In a torsion experiment, loads are applied to the two ends of a cylindrical specimen of radius a and length L, so as to create a torque M about the longitudinal axis (Fig. 6.9a). It is convenient to imagine that the $z = 0$ face is fixed and that the $z = L$ face rotates within its plane by an angle α. A reasonable assumption for the displacement field within the cylinder is that each plane normal to the axis of the cylinder also rotates, by an angle that increases linearly from 0 at $z = 0$ to α at $z = L$. In cylindrical coordinates, this displacement field is

$$u = 0, \quad v = \alpha r z/L, \quad w = 0. \tag{6.15}$$

From (2.275) and (2.280), the stresses and strains associated with these displacements are

$$\varepsilon_{z\theta} = \varepsilon_{\theta z} = \alpha r/2L, \quad \tau_{z\theta} = \tau_{\theta z} = G\alpha r/L, \tag{6.16}$$

with all other stress and strain components vanishing. It is easy to verify that these stresses satisfy the equations of stress equilibrium, (5.107)–(5.109), and also give zero tractions along the outer surface of the cylinder, $r = a$. The total moment applied to the end of the cylinder, about the z-axis, is found from

$$M = \int_0^a \int_0^{2\pi} \tau_{z\theta} r^2 \mathrm{d}r\mathrm{d}\theta = \frac{2\pi G\alpha}{L} \int_0^a r^3 \mathrm{d}r = \frac{\pi G a^4 \alpha}{2L}. \tag{6.17}$$

Hence, measurement of M and α will allow G to be found.

Elimination of G between (6.16) and (6.17) yields $\tau_{z\theta} = 2Mr/\pi a^4$, which shows that the shear stresses within the cylinder vary from 0 at the center of

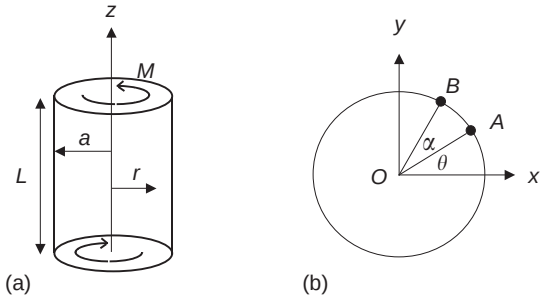

Fig. 6.9 (a) Torsion of a circular cylinder by moments applied over the opposing faces; (b) view of the $z = L$ face, showing rotation of point A to point B by angle α.

the cylinder, to a maximum of $\tau_{z\theta} = 2M/\pi a^3$ at the outer surface. At the outer surface, the principal stresses are, from (2.37)–(2.38), seen to be $\pm 2M/\pi a^3$.

More complex, but predictable, stress fields can be obtained using hollow cylinders. Talesnick and Ringel (1999) developed an apparatus that can apply torsion to a hollow cylinder, superposed on a traditional triaxial stress state, and used it to determine the five independent elastic moduli of several transversely isotropic rocks: Loveland sandstone, Indiana limestone, Lac du Bonnet granite, and Marasha chalk. Paterson and Olgaard (2000) developed an apparatus that is capable of combining traditional triaxial stresses with large-angle torsion and used it to study the rheological properties of Carrara marble under large shear strains.

6.9 Bending tests

Bending is used in rock testing, for measurement of E and for tensile strength (Pomeroy and Morgans, 1956; Berenbaum and Brodie, 1959; Evans, 1961; Coviello et al., 2005). It is also a very sensitive method for studying creep and transient behavior (Phillips, 1931; Price, 1964). This type of loading produces regions of tensile stress and compressive stress in the rock. The stress and displacement distributions can be found from elementary beam theory, as outlined below.

Consider first a rectangular beam of width b, height h, and length L, as in Fig. 6.10. A moment of magnitude M is applied to the beam about the x-axis. According to the classical Euler–Bernoulli theory, each planar section in the x–y plane remains planar, but rotates about the x-axis, as shown in Fig. 6.10b. Lines of constant-y in the y–z plane, which were initially horizontal, now form circular arcs with C at their center. The upper fibers of the beam, $y > 0$, are in compression, and the lower fibers, $y < 0$, are in tension. The so-called *neutral axis*, $y = 0$, is neither in tension nor compression, so the deformed length of OO' is L and the radius of curvature of the neutral axis is $R = L/\theta$. The deformed length of the upper face of the beam, BB', is $(R - h)\theta$, and its original length was $L = R\theta$, so the longitudinal compressive strain in the upper fibers is $\varepsilon_{zz} = h/R$. Similarly, the strain of the lowermost fibers is $\varepsilon_{zz} = -h/R$. The same analysis for an arbitrary value of y shows that, in general, $\varepsilon_{zz} = y/R$, and so the longitudinal stress is $\tau_{zz} = yE/R$.

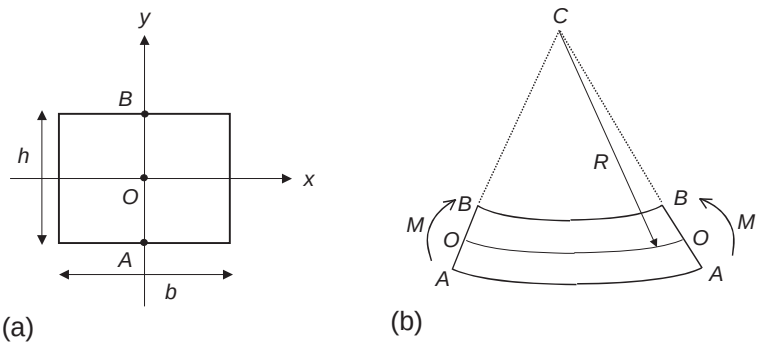

Fig. 6.10 Bending of a prismatic beam by moments applied at its ends: (a) cross section normal to the z-axis; (b) side view, normal to the x-axis.

The total moment about the x-axis is given by

$$M = \int_{-h/2}^{h/2} \int_{-b/2}^{b/2} \tau_{zz} y \mathrm{d}x\mathrm{d}y = \frac{bE}{R} \int_{-h/2}^{h/2} y^2 \mathrm{d}y = \frac{bh^3 E}{12R} \equiv \frac{EI}{R}, \tag{6.18}$$

where $I = bh^3/12$ is the moment of inertia of the cross section, about the x-axis. Measurement of the applied moment and the radius of curvature of the deformed beam therefore provides a value for E. The greatest tensile stress, which occurs at the lower face of the beam, is equal to

$$\tau_{zz}(\text{tensile max}) = -hE/2R = -Mh/2I. \tag{6.19}$$

If the moment is increased until failure occurs, this relation can be used to give the tensile strength.

In practice, the applied loading is somewhat different from the case of pure bending by end-couples. To treat the loading configurations actually used in the laboratory, the following generalization of (6.18) is needed. For small deformations, the radius of curvature can be approximated as $1/R = \mathrm{d}^2y'/\mathrm{d}z^2$, where y' is the deformed position of the neutral axis. The initial position of this axis was $y = 0$, so $y' = v$, where v is the y-component of the displacement of the neutral axis, in which case (6.18) can be written as

$$M = EI \frac{\mathrm{d}^2 v}{\mathrm{d}z^2}. \tag{6.20}$$

This form of the equation can be used for cases in which the moment M varies along the z-axis. The following two cases are of importance in rock mechanics testing.

6.9.1 Three-point loading

Consider a beam that is simply supported at its two ends and loaded by a point load F at its center (Fig. 6.11a). It will be convenient to place the origin at the midpoint of the beam and denote the total length by $2L$. By symmetry, the reaction forces at the two ends will each have magnitude $F/2$. By performing a moment balance on a segment of the beam located between some generic point $0 < z < L$ and the right edge of the beam, it follows that the internal moment acting along the face of the beam, normal to the z-axis, must be

$$M(z) = \tfrac{1}{2}F(L - z). \tag{6.21}$$

The maximum tensile stress occurs again at the lower face of the beam, where it is given by (6.19). According to (6.21), this will occur at the midpoint of the beam, where $z = 0$ and $M_{\max} = FL/2$. Hence, the greatest tensile stress will be

$$\tau_{zz} = -\frac{hFL}{4I}. \tag{6.22}$$

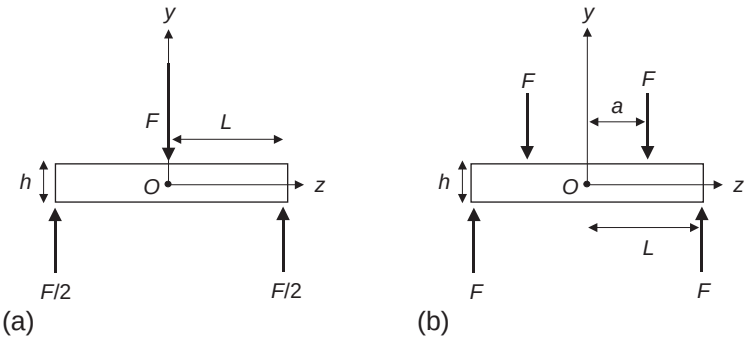

Fig. 6.11
(a) Three-point loading and (b) four-point loading of a beam.

The differential equation (6.20) for the deflection of the beam becomes

$$EI\frac{\mathrm{d}^2v}{\mathrm{d}z^2} = \frac{1}{2}F(L-z). \tag{6.23}$$

Integration of (6.23), using the boundary conditions $v = 0$ and (from symmetry) $\mathrm{d}v/\mathrm{d}z = 0$ when $z = 0$, gives

$$v = \frac{F}{12EI}(3Lz^2 - z^3). \tag{6.24}$$

The displacement at $z = L$ represents the deflection of the midpoint of the beam in the direction of the applied force F:

$$v_{\max} = \frac{FL^3}{6EI}. \tag{6.25}$$

This relation provides a means to estimate E from the deflection of the beam.

6.9.2 Four-point loading

An objection to the use of the three-point loading configuration to estimate tensile strength arises from the fact that the maximum stress (6.22) occurs immediately beneath the point of application of one of the loads, and it is not reasonable to expect elementary beam theory to be very accurate at such locations. This problem can be avoided by using four-point loading (Fig. 6.11b), in which two loads of magnitude F are applied at $z = \pm a$, for some value $0 < a < L$. By symmetry, the reaction forces at the two ends will each have magnitude F. In this case, taking a moment balance for a segment of the beam to the right of the midpoint yields

$$M = F(L-a) \quad \text{for } 0 < z < a, \tag{6.26}$$

$$M = F(L-z) \quad \text{for } a < z < L, \tag{6.27}$$

with similar expressions for the region $z < 0$. Hence, the moment is uniform and equal to $F(L-a)$ throughout the entire region $-a < z < a$. So, the magnitude of the maximum tensile stress is

$$|\tau_{zz}|_{\max} = \frac{Mh}{2I} = \frac{Fh(L-a)}{2I}. \tag{6.28}$$

In particular, this stress will occur at the midpoint of the beam, $z = 0$, which is not located immediately under any of the concentrated loads.

The maximum deflection of beam can be calculated in this case to be

$$v_{\max} = \frac{F}{6EI}(2L^3 - 3a^2L + a^3). \tag{6.29}$$

The theory described above assumes linear elastic behavior of the rock. Exadaktylos et al. (2001a,b) gave an analysis of bending that accounted for nonlinearity in the stress–strain behavior and also for the possibility that the elastic modulus E may be different in tension than in compression. The model was applied to three-point bending tests conducted on a Dionysos marble, for which $E_c = 0.8E_t$. They found that tensile failure occurred at the lower edge of the beam, at a (local) stress that was consistent with the tensile strength measured under direct uniaxial tension.

6.10 Hollow cylinders

A hollow cylinder subjected to an axial load and an external or internal fluid pressure along its curved surfaces provides a ready method for studying the strength and fracture of rock under a variety of principal stresses. Among the earliest tests on hollow cylinders of rock were those of Adams (1912), who observed failure by spalling at the inner surface of the cylinder. His results, along with some of their geological implications, were discussed by King (1912). Robertson (1955) used cylinders of rock with different ratios of their inner and outer diameter, stressed by fluid pressure applied to their ends and outer surfaces. He discussed his results, in which failure started at the inner surface, in terms of elastic–plastic theory. Hollow cylinders subjected to axial load and external fluid pressure have been used since then on a variety of rock types (Hobbs, 1962; Obert and Stephenson, 1965; Santarelli and Brown, 1989; Lee et al., 1999).

The solutions for the stresses in a pressurized hollow cylinder are given in §8.4. Consider first the case of a hollow cylinder of inner radius, a, and outer radius, b, subjected to a compressive axial stress, σ, and an external fluid pressure, p_o. At the inner surface, the three principal stresses will be

$$\tau_{zz} = \sigma, \quad \tau_{\theta\theta} = 2p_o/(1 - \rho^2), \quad \tau_{rr} = 0, \tag{6.30}$$

and at the outer surface, the principal stresses will be

$$\tau_{zz} = \sigma, \quad \tau_{\theta\theta} = p_o(1 + \rho^2)/(1 - \rho^2), \quad \tau_{rr} = p_o, \tag{6.31}$$

where $\rho = a/b$. The axial stress is the same at both surfaces, and as $\rho < 1$ by definition, it follows that the maximum and minimum principal stresses will always occur at the inner surface, where the minimum principal stress is zero. Depending on the numerical values of σ and p_o, the maximum principal stress may be either τ_{zz} or $\tau_{\theta\theta}$. According to the common failure theories discussed in Chapters 4 and 10, this specimen would be expected to fail at its inner surface, at a value of the maximum principal stress that differs from the uniaxial strength

of the rock by the strengthening influence, if any, of the intermediate principal stress.

If $\sigma > 2p_o/(1-\rho^2)$, then the principal stresses at the inner surface of the cylinder are

$$\sigma_1 = \sigma, \quad \sigma_2 = 2p_o/(1-\rho^2), \quad \sigma_3 = 0. \tag{6.32}$$

For relatively small values of the outer confining pressure p_o and the inner radius a, failure will occur much as it does for a solid cylinder under triaxial compression, forming a single shear fracture across the entire cylinder at some small angle to the longitudinal axis (Fig. 6.12a). For larger values of p_o and a, failure will occur in the form of a conical fracture whose axis lies along that of the cylinder (Fig. 6.12b). The conical fracture surface will be tangential to the direction of the intermediate principal stress (i.e., the θ direction).

If $\sigma < 2p_o/(1-\rho^2)$, then the principal stresses at the inner surface of the cylinder are

$$\sigma_1 = 2p_o/(1-\rho^2), \quad \sigma_2 = \sigma, \quad \sigma_3 = 0. \tag{6.33}$$

In this case, failure occurs by spiral fractures that are parallel to the axis of the cylinder and consequently parallel to the direction of the intermediate principal stress (Fig. 6.12c).

Consider now a hollow cylinder subjected to an internal pressure p_i along its inner surface and an axial stress σ. If $\sigma < p_i$, the principal stresses at the inner surface are

$$\sigma_1 = \tau_{rr} = p_i, \quad \sigma_2 = \tau_{zz} = \sigma, \quad \sigma_3 = \tau_{\theta\theta} = -p_i(1+\rho^2)/(1-\rho^2), \tag{6.34}$$

and failure usually occurs as a planar, diametral extension fracture. If $\sigma > p_i$, the principal stresses at the inner surface are

$$\sigma_1 = \tau_{zz} = \sigma, \quad \sigma_2 = \tau_{rr} = p_i, \quad \sigma_3 = \tau_{\theta\theta} = -p_i(1+\rho^2)/(1-\rho^2). \tag{6.35}$$

In this case the intermediate principal stress is radial and helicoidal fractures are observed.

In the general case, both internal and external pressures can be applied to the cylinder, along with an axial stress. By using various combinations of σ, p_i,

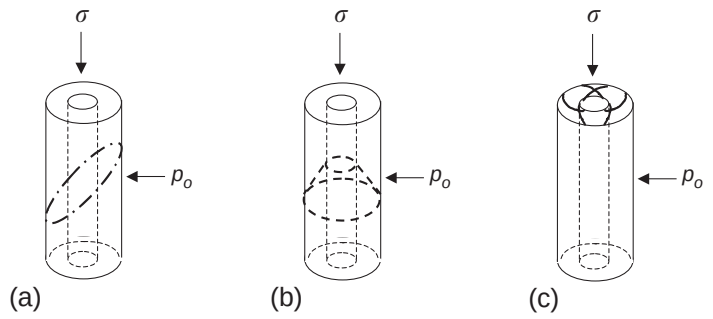

Fig. 6.12 Different systems of fracture in a hollow cylinder subjected to axial stress and external pressure (see text for details).

and p_o, large regions of the failure surface $\sigma_1 = f(\sigma_2, \sigma_3)$ can be probed. Alsayed (2002) modified a traditional Hoek triaxial cell (Hoek and Franklin, 1968) so as to accept hollow cylinders and used it to study the behavior of Springwell sandstone under a variety of stress conditions. Hollow cylinder tests such as those described above are of particular value in the analysis of borehole stability problems (Ewy et al., 2001).